Papers, volume 5 - 1997-2000

Thoft-Christensen, Palle

Publication date:
2006

Document Version
Publisher's PDF, also known as Version of record

Link to publication from Aalborg University

Citation for published version (APA):
Thoft-Christensen, P. (2006). *Papers, volume 5 - 1997-2000*. Aalborg Universitetsforlag.

CHAPTER 105

SUSPENSION BRIDGE FLUTTER FOR GIRDERS WITH SEPARATE CONTROL FLAPS[1]

T. Huynh & P. Thoft-Christensen
Aalborg University, Aalborg, Denmark

ABSTRACT

Active vibration control of long span suspension bridge flutter using separated control flaps (SFSC) has shown to increase effectively the critical wind speed of the bridges. In this paper, an SFSC calculation based on modal equations of the vertical and torsional motions of the bridge girder including the flaps is presented. The length of the flaps attached to the girder, the flap configuration, and the flap rotational angles are parameters used to increase the critical wind speed of the bridge. To illustrate the theory a numerical example is shown for a suspension bridge of 1000m + 2500m + 1000m span based on the Great Belt Bridge streamlined girder.

1. INTRODUCTION

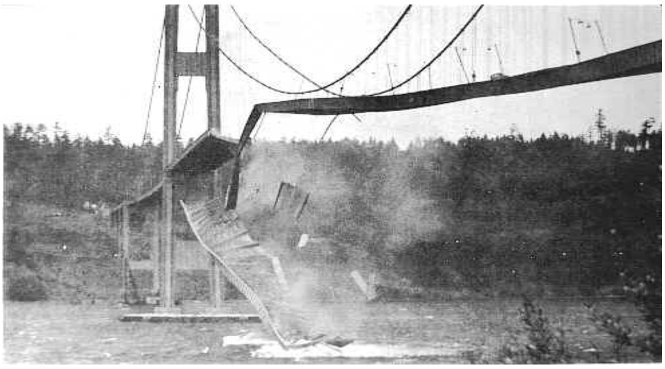

Figure 1.Tacoma Narrows Bridge Collapse (1940)

The motion-induced wind loads on bridges have in many cases been transformed into catastrophic forces. As examples, mention can be made of the destruction of the Brighton Chain Pier suspension bridge (1836), the Ohio River Bridge, (West Virginia 1854) and the well-known Tacoma Narrows Bridge (1940), see figure 1.

[1] Journal of Bridge Engineering, Vol. 6, 2001, pp. 168-175.

There are three main reasons for these dynamic collapses: (1) Aerodynamic instability (negative damping) producing self-induced vibrations in the structure, (2) Eddy formations, which might be periodic in nature, and (3) Random effects of turbulence, i.e. the random fluctuations in velocity and direction of the wind. These three subjects have been important topics within suspension bridge aerodynamic stability research for the last 60 years. A relatively new research area on aerodynamic stability for very long-span bridges is based on actively controlled flaps attached along the girders, Ostenfeld & Larsen [1]. The purpose of applying the so-called control flaps is that the small rotations of the flaps attached along the girder in strong wind will generate the aeroelastic forces to counteract the aeroelastic forces occurred from the girder vibration. Two designs for the control flaps have been the revolving "wind nose" as the integrated parts of the girder and the separated flaps attached under the girder, see figure 4. Hansen & Thoft-Christensen [2], [3] and Hansen [4] have investigated the first-mentioned design. This paper deals with the last-mentioned design.

2. SUSPENSION BRIDGE FLUTTER

Let $v_z(x,t)$ be the vertical displacement along the girder in mode i, and $r_x(x,t)$ the torsional displacement in mode j, both coupled to produce a flutter mode at the time t, see figure 2

$$v_z(x,t) = \phi_i(x) z_i(t) \quad (1)$$

$$r_x(x,t) = \psi_j(x) \alpha_j(t) \quad (2)$$

where $\phi_i(x)$ and $\psi_j(x)$ are the vertical mode i and the torsional mode j at the joint x on the girder, respectively. $z_i(t)$ and $\alpha_j(t)$ are the associated modal coordinates in the modes i and j.

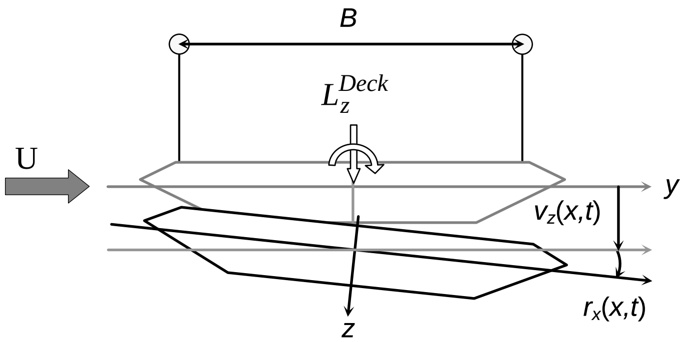

Figure 2. Vertical and torsional displacements of the girder section

The motion-induced forces due to the movement of the girder in the coupled vertical-tosional mode k can be written, Scanlan (1996)

$$L_z^{deck}(x,t) = \frac{\rho U^2 B}{2}\left[\frac{KH_1^*(K)}{U}\dot{v}_z + \frac{KH_2^*(K)B}{U}\dot{r}_x + K^2 H_3^*(K) r_x + \frac{K^2 H_4^*(K)}{B} v_z\right] \quad (3)$$

$$M_x^{deck}(x,t) = \frac{\rho U^2 B^2}{2}\left[\frac{KA_1^*(K)}{U}\dot{v}_z + \frac{KA_2^*(K)B}{U}\dot{r}_x + K^2 A_3^*(K) r_x + \frac{K^2 A_4^*(K)}{B} v_z\right] \quad (4)$$

where $K = B\omega/U$ is the reduced frequency, B is the girder width, U is the uniform approach velocity of the wind, and ω is the bridge circular frequency of oscillation at the wind action U. $H_i^*(K)$ and $A_i^*(K)$, i=1,2,3,4 are the flutter derivatives determined experimentally in a wind tunnel.

The modal wind load and the modal mass due to a coupled vertical-torsional mode k are

$$F_k^{deck}(t)=\int_0^L [\,\phi_k(x)\quad \psi_k(x)]\begin{bmatrix} L_z^{deck}(x,t)\\ M_x^{deck}(x,t)\end{bmatrix}dx \tag{5}$$

$$M_k=\int_0^L [\,\phi_k(x)\quad \psi_k(x)]\begin{bmatrix} m & 0\\ 0 & J\end{bmatrix}\begin{bmatrix}\phi_k(x)\\ \psi_k(x)\end{bmatrix}dx \tag{6}$$

where m and J are the mass and the mass moment of inertia per unit span including cables. Each of integral (5) and (6) is a sum of three integrals, namely, two for the side spans of the lengths L_s and one for the main span of the length L_m. The corresponding mode shapes $\phi_{s,k}(x)$, $\psi_{s,k}(x)$ of the side spans, and $\phi_{m,k}(x)$, $\psi_{m,k}(x)$ of the main span are given in the Appendix.

$$\begin{aligned} F_z^{deck}(t)=\frac{\rho U^2 B}{2}\Bigg[&\frac{KH_1^*(K)\,\Phi}{U}\dot{z}_1(t)+\frac{KH_2^*(K)B\Xi}{U}\dot{\alpha}_1(t)\\ &+K^2H_3^*(K)\,\Xi\alpha_1(t)+\frac{K^2H_4^*(K)\,\Phi}{B}z_1(t)\Bigg]\end{aligned} \tag{7}$$

$$\begin{aligned} F_x^{deck}(t)=\frac{\rho U^2 B^2}{2}\Bigg[&\frac{KA_1^*(K)\,\Xi}{U}\dot{z}_1(t)+\frac{KA_2^*(K)B\Psi}{U}\dot{\alpha}_1(t)\\ &+K^2A_3^*(K)\,\Psi\alpha_1(t)+\frac{K^2A_4^*(K)\,\Xi}{B}z_1(t)\Bigg]\end{aligned} \tag{8}$$

where

$$\Phi=\int_0^L \phi_1^2(x)dx\ ,\ \Xi=\int_0^L \phi_1(x)\psi_1(x)dx\ ,\ \text{and}\quad \Psi=\int_0^L \psi_1^2(x)dx \tag{9}$$

and where (3) and (4) have been inserted. $\phi_i\equiv\phi_k\equiv\phi_1$ for the 1st symmetric vertical (SV1) mode, and $\psi_j\equiv\psi_k\equiv\psi_1$ for the 1st symmetric torsional (ST1) mode are assumed to couple at the flutter mode. In the short form, (7) and (8) can be written as:

$$F_z^{deck}(t)=H1\,\dot{z}_1(t)+H2\,\dot{\alpha}_1(t)+H3\,\alpha_1(t)+H4\,z_1(t) \tag{10}$$

$$F_x^{deck}(t)=A1\,\dot{z}_1(t)+A2\,\dot{\alpha}_1(t)+A3\,\alpha_1(t)+A4\,z_1(t) \tag{11}$$

where

$$\begin{bmatrix}H1\\ H2\\ H3\\ H4\end{bmatrix}=\frac{\rho UBK}{2}\begin{bmatrix}H_1^*\Phi\\ BH_2^*\Xi\\ UKH_3^*\Xi\\ \dfrac{UK}{B}H_4^*\Phi\end{bmatrix} \tag{12}$$

$$\begin{bmatrix}A1\\ A2\\ A3\\ A4\end{bmatrix}=\frac{\rho UB^2K}{2}\begin{bmatrix}A_1^*\Xi\\ BA_2^*\Psi\\ UKA_3^*\Psi\\ \dfrac{UK}{B}A_4^*\Xi\end{bmatrix} \tag{13}$$

The modal mass at the pure vertical mode and the pure torsional mode is, cf. (6)

$$M_z = \int_0^L m\phi_1^2(x)dx = m\,\Phi \quad , \quad M_x = \int_0^L J\psi_1^2(x)\,dx = J\,\Psi \tag{14}$$

The governing equations for the vertical-torsional flutter problem are

$$M_z\Big(\ddot{z}(t) + 2\omega_z\zeta_z\dot{z}(t) + \omega_z^2 z(t)\Big) = F_z^{deck} \tag{15}$$

$$M_x\Big(\ddot{\alpha}(t) + 2\omega_\alpha\zeta_\alpha\dot{\alpha}(t) + \omega_\alpha^2\alpha(t)\Big) = F_x^{deck} \tag{16}$$

where ω_z and ζ_z are the natural SV1 frequency (in rad/s) and the associated damping ratio. ω_α and ζ_α are the natural ST1 frequency and the associated damping ratio.

Let both z and α be the temporary dimensionless $s = Ut/B$ at flutter, the following relations are applied, Scanlan (1996)

$$\dot{(\ )} = \frac{d(\ )}{ds}\frac{ds}{dt} = (\ )'\frac{U}{B} \quad , \quad \ddot{(\ )} = \frac{d^2(\ )}{ds^2}\left(\frac{ds}{dt}\right)^2 = (\ )''\frac{U^2}{B^2} \tag{17}$$

Assuming that both z and α at the flutter mode are proportional to $e^{i\omega t}$ where $z(t) = z_0 e^{i\omega t}$ and $\alpha(t) = \alpha_0 e^{i\omega t}$. Setting moreover $Ks = \omega t$, $K_z = B\omega_z/U$, and $K_\alpha = B\omega_\alpha/U$. Using (14) and (17), eqs. (15) and (16) can be written as:

$$\begin{bmatrix} -K^2 + \left(2K_z\zeta_z - \dfrac{K_z H1}{m\omega_z\Phi}\right) iK + \left(K_z^2 - \dfrac{K_z^2 H4}{m\omega_z^2\Phi}\right) - \dfrac{K_\alpha^2 A1U}{J\omega_\alpha^2\Psi}\, iK \\ -\dfrac{K_\alpha^2 BA4}{J\omega_\alpha^2\Psi} - \dfrac{K_z^2 H2U}{m\omega_z^2 B^2\Phi}\, iK - \dfrac{K_z^2 H3}{m\omega_z^2 B\Phi} - K^2 \\ +\left(2K_\alpha\zeta_\alpha - \dfrac{K_\alpha A2}{J\omega_\alpha\Psi}\right) iK + \left(K_\alpha^2 - \dfrac{K_\alpha^2 A3}{J\omega_\alpha^2\Psi}\right) \end{bmatrix} \begin{bmatrix} \dfrac{z}{B} \\ \alpha \end{bmatrix} = \begin{bmatrix} 0 \\ 0 \end{bmatrix} \tag{18}$$

The flutter conditions (the zero determinant for the coefficients of z and α given above) with $H1$ to $H4$ and $A1$ to $A4$ given by (12) and (13) inserted, are

$$\begin{aligned} \mathrm{Re}\big(\mathrm{Det}\big) = {} & \frac{\omega^4}{\omega_z^4}\Bigg[1 + \frac{\rho B^4 A_3^*}{2J} + \frac{\rho B^2 H_4^*}{2m} + \frac{\rho^2 B^6}{4mJ} \\ & \times\left(-H_1^*A_2^* + H_4^*A_3^* + \frac{\Xi\Xi}{\Phi\Psi}\big(-A_4^*H_3^* + A_1^*H_2^*\big)\right)\Bigg] \\ & + \frac{\omega^3}{\omega_z^3}\left[\frac{\rho B^4 A_2^*}{J}\zeta_z + \frac{\rho B^2 H_1^*}{m}\frac{\omega_\alpha}{\omega_z}\zeta_\alpha\right] + \frac{\omega^2}{\omega_z^2}\Bigg[-1 - \frac{\omega_\alpha^2}{\omega_z^2} \\ & - 4\zeta_z\zeta_\alpha\frac{\omega_\alpha}{\omega_z} - \frac{\rho B^4 A_3^*}{2J} - \frac{\rho B^2 H_4^*}{2m}\frac{\omega_\alpha^2}{\omega_z^2}\Bigg] + \frac{\omega_\alpha^2}{\omega_z^2} = 0 \end{aligned} \tag{19}$$

$$\begin{aligned}\mathrm{Im}\left(\mathrm{Det}\right)=&\frac{\omega^3}{\omega_z^3}\left[\frac{\rho B^4 A_2^*}{2J}+\frac{\rho B^2 H_1^*}{2m}+\frac{\rho^2 B^6}{4mJ}\right.\\&\left.\times\left(H_1^* A_3^*+A_2^* H_4^*+\frac{\Xi\Xi}{\Phi\Psi}\left(-A_1^* H_3^*-A_4^* H_2^*\right)\right)\right]\\&+\frac{\omega^2}{\omega_z^2}\left[-2\zeta_z-2\zeta_\alpha\frac{\omega_\alpha}{\omega_z}-\zeta_\alpha\frac{\rho B^2 H_4^*}{m}\frac{\omega_\alpha}{\omega_z}-\zeta_z\frac{\rho B^4 A_3^*}{J}\right]\\&+\frac{\omega}{\omega_z}\left[-\frac{\rho B^4 A_2^*}{2J}-\frac{\rho B^2 H_1^*}{2m}\frac{\omega_\alpha^2}{\omega_z^2}\right]+2\zeta_z\frac{\omega_\alpha^2}{\omega_z^2}+2\zeta_\alpha\frac{\omega_\alpha}{\omega_z}=0\end{aligned}\tag{20}$$

U_{cr} and ω_{cr} can be found directly by graphical iteration using Maple V and Matlab :

(1) Use MatLab to express the flutter derivatives $H_i^*(U,\omega)$ and $A_i^*(U,\omega)$ in the polynomial of U and ω based on e.g. measured values from wind tunnel tests.

(2) Express Re(*Det*) and Im(*Det*) in one unknown ω for a prediction of U, where ω_z, ω_α , ζ_z , ζ_α , ρ, m, J, and B all are constants. For a prediction of U, Re(*Det*) and Im(*Det*) are plotted by Maple V as a function of ω. The flutter solution ω_{cr} is found where Re(*Det*) and Im(*Det*) are intersecting on the ω-axis ($\omega_z < \omega_{cr} < \omega_\alpha$) and U_{cr} is the last U predicted. (For a predicted $U < U_{cr}$, the intersection will be below the ω-axis and vice versa, see the numerical example in section 4).

The suspension bridge flutter conditions (19) and (20) are also known as the sectional flutter conditions when setting $\Xi\Xi = \Phi\Psi = 1$, i.e. the first SV and ST mode shapes are equal to a constant mode shape indicating a possible mode coupling. In the case of a full-span bridge, the deformations of the girder are functions of the position along the girder axis so that the sectional assumption is no longer valid, especially when the deformations (mode shapes) of the flaps along the girder are taking into account in the flutter conditions.

For multi-mode flutter (depends on the bridge design, the natural mode shapes and its frequencies) the governing flutter equations (15) and (16) are increased to a number of equations according to the number of modes, say m modes. Hence, the determinant condition (18) becomes of the dimension $m\times m$. In case of the Great Belt Bridge, a two-mode flutter analysis consisting of the SV1 and the ST1 mode gives a almost unchanged results compared to a four-mode analysis including the SV2 and ST2 modes, Nielsen & Huynh [5].

Figure 3. The Great Belt Bridge (1998)

3. SUSPENSION BRIDGE FLUTTER FOR GIRDER WITH SEPARATED CONTROL FLAPS (SFSC)

The aeroelastic forces occur from the girder cross-section and the flaps are as shown in figure 4. The system is assumed to oscillate from position B to C. The total aeroelastic forces on the girder and on the flaps are

$$L_z^{total} = L_z^{Deck} + L_z^{tr}(v_z, r_x^{tr}) + L_z^{le}(v_z, r_x^{le}) \tag{21)}$$

$$M_x^{total} = M_x^{Deck} + M_x^{tr}(v_z, r_x^{tr}) + M_x^{le}(v_z, r_x^{le}) + \left(L_z^{tr}(v, r_x^{tr}) - L_z^{le}(-v, r_x^{le})\right)\frac{B}{2} \tag{22}$$

where $r_x^{le}(x,t)$ and $r_x^{tr}(x,t)$ are the leading and trailing flap rotations from horizontal position. $L_z^{le}(v_z, r_x^{le})$ and $L_z^{tr}(v_z, r_x^{tr})$ are the lift-induced forces from the leading and trailing flaps. $M_x^{le}(v_z, r_x^{le})$ and $M_x^{tr}(v_z, r_x^{tr})$ are the moment-induced forces from the leading and trailing flaps. $v(x,t) = r_x(x,t)B/2$ is the vertical displacement of the flaps due to the girder rotation r_x. $L_z^{tr}(v, r_x^{tr})B/2$ and $L_z^{le}(-v, r_x^{tr})B/2$ are the moment-induced forces from the lift of the leading and trailing flaps due to the vertical displacement $v(x,t)$.

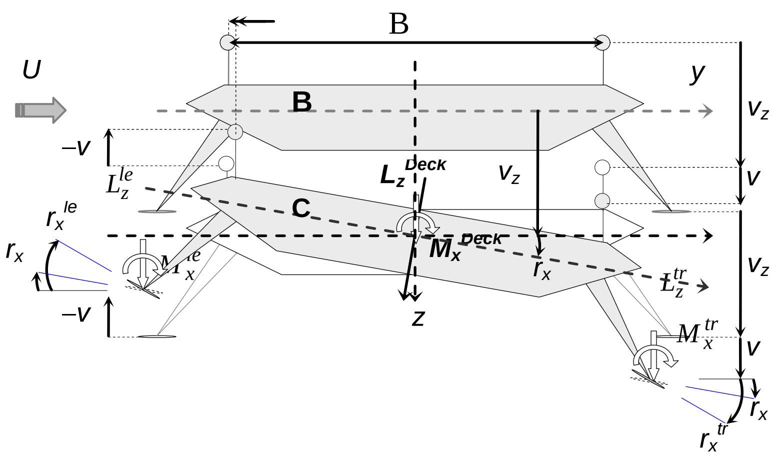

Figure 4. Motion-induced wind loads on the girder and on the flaps

When the system oscillates purely vertically, the vertical displacements of the flaps at location x are the same as the girder vertical displacement at the same location:

$$v_{z,i}^{tr}(x,t) = v_{z,i}^{le}(x,t) = v_{z,i}(x,t) = \phi_i(x) z_i(t) \tag{23}$$

When the system oscillates purely torsional, the rotations of the flaps at location x are assumed to be a_{tr} and a_{le} times the rotation of the girder $r_{x,j}(x,t)$ (by external power)

$$\begin{bmatrix} r_{x,j}^{le} \\ r_{x,j}^{tr} \end{bmatrix} = \begin{bmatrix} a_{le} \\ a_{tr} \end{bmatrix} r_{x,j} = \begin{bmatrix} a_{le} \\ a_{tr} \end{bmatrix} \psi_j(x) \alpha_j(t) \tag{24}$$

where a_{tr} and a_{le} are the rotational amplification factor of the trailing and leading flaps, respectively. $a_{tr} = a_{le} = 1$ indicates that $r_x^{tr} = r_x^{le} = r_x$ i.e. the flap rotations are the same as the girder rotation.

The vertical translation $v(x,t)$ due to a small girder rotation $r_x(x,t)$ is

$$v(x,t)=\frac{B}{2}r_x(x,t)=\frac{B}{2}\psi_j(x)\alpha_j(t) \tag{25}$$

The aeroelastic from the flaps caused by v_z and the flaps rotations are

$$\begin{bmatrix} L_z^{le}(v_z,r_x^{le}) \\ L_z^{tr}(v_z,r_x^{tr}) \end{bmatrix}=\frac{\rho U^2 B' K'}{2}\left\{\frac{H_5^*(K')}{U}\dot{v}_z\begin{bmatrix}1\\1\end{bmatrix}+\frac{H_6^*(K')B'}{U}\begin{bmatrix}\dot{r}_x^{le}\\ \dot{r}_x^{tr}\end{bmatrix}\right.$$

$$\left.+K'H_7^*(K')\begin{bmatrix}r_x^{le}\\ r_x^{tr}\end{bmatrix}+\frac{K'H_8^*(K')}{B'}v_z\begin{bmatrix}1\\1\end{bmatrix}\right\} \tag{26}$$

$$\begin{bmatrix} M_x^{le}(v_z,r_x^{le}) \\ M_x^{tr}(v_z,r_x^{tr}) \end{bmatrix}=\frac{\rho U^2 B'^2 K'}{2}\left\{\frac{A_5^*(K')}{U}\dot{v}_z\begin{bmatrix}1\\1\end{bmatrix}+\frac{A_6^*(K')B'}{U}\begin{bmatrix}\dot{r}_x^{le}\\ \dot{r}_x^{tr}\end{bmatrix}\right.$$

$$\left.+K'A_7^*(K')\begin{bmatrix}r_x^{le}\\ r_x^{tr}\end{bmatrix}+\frac{K'A_8^*(K')}{B'}v_z\begin{bmatrix}1\\1\end{bmatrix}\right\} \tag{27}$$

The lift forces from the flaps caused by v and the flaps rotation are

$$\begin{bmatrix} L_z^{le}(-v,r_x^{le}) \\ L_z^{tr}(v,r_x^{tr}) \end{bmatrix}=\frac{\rho U^2 B' K'}{2}\left\{\frac{H_5^*(K')}{U}\dot{v}\begin{bmatrix}-1\\1\end{bmatrix}+\frac{H_6^*(K')B'}{U}\begin{bmatrix}\dot{r}_x^{le}\\ \dot{r}_x^{tr}\end{bmatrix}\right.$$

$$\left.+K'H_7^*(K')\begin{bmatrix}r_x^{le}\\ r_x^{tr}\end{bmatrix}+\frac{K'H_8^*(K')}{B'}v\begin{bmatrix}-1\\1\end{bmatrix}\right\} \tag{28}$$

where

$$K'=B'\omega/U \tag{29}$$

and where B' is the width of the flaps (e.g. 10% of the girder width). The flap flutter derivatives $H_i^*(K')$ and $A_i^*(K')$, I = 5, 6, 7, 8 given by Simiu & Scanlan [7] are

$$K'H_5^*=-2\pi F \qquad K'A_5^*=\frac{\pi F}{2} \tag{30}$$

$$K'H_6^*=-\frac{\pi}{2}\left[1+\frac{4G}{K'}+F\right] \qquad K'A_6^*=-\frac{\pi}{2K'}\left[\frac{K'}{4}-G-\frac{K'F}{4}\right] \tag{31}$$

$$K'^2H_7^*=-\pi\left[2F-\frac{GK'}{2}\right] \qquad K'^2A_7^*=\frac{\pi}{2}\left[\frac{K'^2}{32}+F-\frac{K'G}{4}\right] \tag{32}$$

$$K'^2H_8^*=\frac{\pi K'^2}{2}\left[1+\frac{4G}{K'}\right] \qquad K'^2A_8^*=-\frac{\pi K'G}{2} \tag{33}$$

and where $F(k')$ and $G(k')$ are known as the real and the imaginary parts of the Theodorsen circulation function $C(k')$ given by (Theodorsen Function Exact Values for $k'\in[0-1.4]$ expressed in polynomial with the third correct decimal, using MatLab)

$$F(k')=\frac{537}{1039}k'^6-\frac{1533}{547}k'^5+\frac{2642}{423}k'^4-\frac{3399}{457}k'^3+\frac{1847}{357}k'^2-\frac{4299}{1990}k'+\frac{1377}{1372} \tag{34}$$

$$G(k')=\frac{11549}{45}k'^{12}-\frac{41019}{19}k'^{11}+\frac{72058}{9}k'^{10}-\frac{206821}{12}k'^9+\frac{572785}{24}k'^8-\frac{289524}{13}k'^7$$

$$+\frac{157031}{11}k'^6-\frac{25197}{4}k'^5+\frac{24646}{13}k'^4-\frac{26462}{69}k'^3+\frac{2941}{57}k'^2-\frac{7121}{1617}k'-\frac{207}{69064} \tag{35}$$

where

$$k' = B'\omega/2U = K'/2 \tag{36}$$

4. MODAL WIND LOADS ON THE FLAPS AND SFSC

The modal wind loads from the flaps are

$$F_z^{tr}(t) + F_z^{le}(t) = \int_{L_1}^{L_2} \left(L_z^{tr}(v_z, r_x^{tr}) + L_z^{le}(v_z, r_x^{le}) \right) \phi_i(x)\, dx \tag{37}$$

$$F_x^{tr}(t) + F_x^{le}(t) = \int_{L_1}^{L_2} \left(M_x^{tr}(v_z, r_x^{tr}) + M_x^{le}(v_z, r_x^{le}) \right) \psi_j(x)\, dx \tag{38}$$

$$F_{xz}^{tr}(t) - F_{xz}^{le}(t) = \int_{L_1}^{L_2} \left(L_z^{tr}(v, r_x^{tr}) - L_z^{le}(-v, r_x^{le}) \right) \frac{B}{2} \psi_j(x)\, dx \tag{39}$$

where (39) is the moment contribution of the leading and trailing flaps due to the rotation of the flaps and due to the vertical translation $v(x,t)$ when the girder rotates. The total lift and torque from the flaps can be written, when (26) to (28) have been inserted into (37) to (39)

$$F_z^{tr}(t) + F_z^{le}(t) = F1\,\dot{z}_i + F2\,\dot{\alpha}_j + F3\,\alpha_j + F4\,z_i \tag{40}$$

$$F_x^{tr}(t) + F_x^{le}(t) + F_{xz}^{tr}(t) - F_{xz}^{le}(t) = T1\dot{z}_i + T2\,\dot{\alpha}_j + T3\,\alpha_j + T4 z_i \tag{41}$$

where

$$F1 = -\rho U 2B'\pi\, F\Phi_f \tag{42}$$

$$F2 = -\frac{\rho U B'^2 \pi}{4} \left(1 + \frac{4G}{K'} + F\right) (a_{tr} + a_{le}) \Xi_f \tag{43}$$

$$F3 = -\frac{\rho U^2 B'\pi}{2} \left(2F - \frac{GK'}{2}\right) (a_{tr} + a_{le}) \Xi_f \tag{44}$$

$$F4 = \frac{\rho U^2 \pi K'^2}{2} \left(1 + \frac{4G}{K'}\right) \Phi_f \tag{45}$$

$$T1 = \frac{\rho U B'^2 \pi F}{2} \Xi_f \tag{46}$$

$$T2 = \frac{\rho U B'^2 \pi}{2} \left[-B' \left(\frac{1}{8} - \frac{G}{2K'} - \frac{F}{8} \right) (a_{tr} + a_{le}) + \frac{B}{B'} \left(-FB + \frac{B'}{4} \left(1 + \frac{4G}{K'} + F\right) (a_{le} - a_{tr}) \right) \right] \Psi_f \tag{47}$$

$$T3 = \frac{\rho U^2 B'^2 \pi}{4} \left[\left(\frac{K'^2}{32} + F - \frac{K'G}{4} \right) (a_{tr} + a_{le}) + \frac{B}{B'} \left(\left(2F - \frac{GK'}{2} \right) (a_{le} - a_{tr}) + \frac{K'^2 B}{2B'} \left(1 + \frac{4G}{K'} \right) \right) \right] \Psi_f \tag{48}$$

$$T4 = -\frac{\rho U^2 B' \pi\, K'G}{2} \Xi_f \tag{49}$$

and where the lengths $|L_2 – L_1|$ of the flaps are entered into the modal wind loads in the integrals

$$\Phi_f = \int_{L_1}^{L_2} \phi_1^2(x)dx \quad , \quad \Xi_f = \int_{L_1}^{L_2} \psi_1(x)\phi_1(x)dx \quad , \quad \Psi_f = \int_{L_1}^{L_2} \psi_1^2(x)dx \tag{50}$$

The total modal wind loads on the girder including the flaps are

$$F_z^{deck} + F_z^{tr} + F_z^{le} = L1\,\dot{z}_i + L2\,\dot{\alpha}_j + L3\,\alpha_j + L4\,z_i \tag{51}$$

$$F_x^{deck} + F_x^{tr} + F_x^{le} + F_{xz}^{tr} - F_{xz}^{le} = M1\,\dot{z}_i + M2\,\dot{\alpha}_j + M3\,\alpha_j + M4\,z_i \tag{52}$$

where

$$L1 = H1 + F1 \qquad M1 = A1 + T1 \tag{53}$$

$$L2 = H2 + F2 \qquad M2 = A2 + T2 \tag{54}$$

$$L3 = H3 + F3 \qquad M3 = A3 + T3 \tag{55}$$

$$L4 = H4 + F4 \qquad M4 = A4 + T4 \tag{56}$$

and where $H1$ to $H4$, $A1$ to $A4$ are given by (12) and (13).

Returning to the governing equations without the flaps (15), (16) and (10), (11) it is seen that $L1$ to $L4$ now replace $H1$ to $H4$, and $M1$ to $M4$ replace $A1$ to $A4$. Thus, the SFSC conditions can be written in the form of (19) and (20) as

$$\begin{aligned}\mathrm{Re}(Det) = {} & \frac{\omega^4}{\omega_z^4}\left(1 + \frac{\mathcal{M}_3}{J\omega^2} + \frac{1}{mJ\omega^4}\left[-\omega^2 \mathcal{L}_1\mathcal{M}_2 + \mathcal{L}_2\mathcal{M}_3\right.\right. \\ & \left.\left. -\mathcal{M}_4\mathcal{L}_3 + \omega^2 \mathcal{M}_1\mathcal{L}_2\right] + \frac{\mathcal{L}_4}{m\omega^2}\right) + \frac{\omega^3}{\omega_z^3}\left(2\zeta_z \frac{\mathcal{M}_2}{J\omega} + 2\zeta_\alpha \frac{\omega_\alpha}{\omega_z}\frac{\mathcal{L}_1}{m\omega}\right) \\ & + \frac{\omega^2}{\omega_z^2}\left(-1 - \frac{\omega_\alpha^2}{\omega_z^2} - 4\frac{\omega_\alpha}{\omega_z}\zeta_z\zeta_\alpha - \frac{\mathcal{M}_3}{J\omega^2} - \frac{\omega_\alpha^2}{\omega_z^2}\frac{\mathcal{L}_4}{m\omega^2}\right) + \frac{\omega_\alpha^2}{\omega_z^2} = 0\end{aligned} \tag{57}$$

$$\begin{aligned}\mathrm{Im}(Det) = {} & \frac{\omega^3}{\omega_z^3}\left(\frac{\mathcal{M}_2}{J\omega} + \frac{1}{mJ\omega^3}\left[\mathcal{L}_1\mathcal{M}_3 + \mathcal{L}_4\mathcal{M}_2 - \mathcal{M}_1\mathcal{L}_3\right.\right. \\ & \left.\left. - \mathcal{M}_4\mathcal{L}_2\right] + \frac{\mathcal{L}_1}{m\omega}\right) + \frac{\omega^2}{\omega_z^2}\left(-2\zeta_z - 2\zeta_\alpha\frac{\omega_\alpha}{\omega_z}\frac{\mathcal{L}_4}{m\omega^2} - 2\zeta_z\frac{\mathcal{M}_3}{J\omega^2}\right. \\ & \left. -2\zeta_\alpha\frac{\omega_\alpha}{\omega_z}\right) + \frac{\omega}{\omega_z}\left(-\frac{\mathcal{M}_2}{J\omega} - \frac{\omega_\alpha^2}{\omega_z^2}\frac{\mathcal{L}_1}{m\omega}\right) + 2\zeta_z\frac{\omega_\alpha^2}{\omega_z^2} + 2\zeta_\alpha\frac{\omega_\alpha}{\omega_z} = 0\end{aligned} \tag{58}$$

where

$$\mathcal{L}_1 = \frac{L1}{\Phi} \qquad \mathcal{L}_4 = \frac{L4}{\Phi} \qquad \mathcal{M}_2 = \frac{M2}{\Psi} \tag{59}$$

$$\mathcal{M}_3 = \frac{M3}{\Psi} \qquad \mathcal{L}_1\mathcal{M}_2 = \frac{L1M2}{\Phi\Psi} \qquad \mathcal{L}_4\mathcal{M}_3 = \frac{L4M3}{\Phi\Psi} \tag{60}$$

$$\mathcal{M}_4\mathcal{L}_3 = \frac{M4L3}{\Psi\Phi} \qquad \mathcal{M}_1\mathcal{L}_2 = \frac{M1L2}{\Phi\Psi} \qquad \mathcal{L}_1\mathcal{M}_3 = \frac{L1M3}{\Phi\Psi} \tag{61}$$

$$\mathcal{L}_4\mathcal{M}_2 = \frac{L4M2}{\Phi\Psi} \qquad \mathcal{M}_1\mathcal{L}_3 = \frac{M1L3}{\Phi\Psi} \qquad \mathcal{M}_4\mathcal{L}_2 = \frac{M4L2}{\Phi\Psi} \tag{62}$$

5. NUMERICAL EXAMPLE

Suspension bridge and flutter example

To illustrate the theory a numerical example is shown for the bridge in figure 5. The bridge data are:

- Main span length L_m= 2500 m
- Side span length L_s = 1000 m
- Cable sag in main span f_m = 265 m
- Cable area (one main cable) A_c= 0.56 m^2
- Cable mass (one main cable) m_c= 4396 kg/m
- Cable space B= 27 m
- Girder mass m_g= 14908 kg/m
- Girder mass mom. of inertia J_g = 2.5 E6 kgm^2/m
- Youngs modulus E= 2.1 E11 N/m^2
- Shear modulus G= 0.808 E11 N/m^2
- Air density ρ= 1.29 kg/m^3
- Struc. damp. of SV and ST mode= 0.02

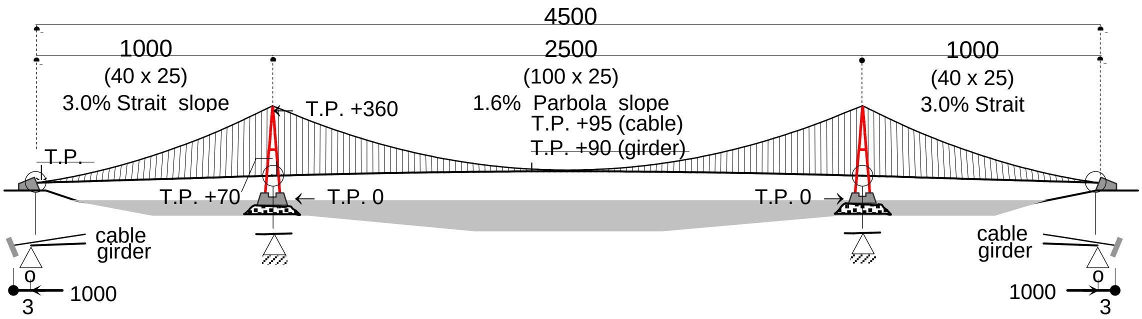

Figure 5. Design example, status supports and dimension in m

Figure 5 shows the main structure of the suspension bridge. The streamlined girder of the Great Belt Bridge is used as input member data. Figure 6 shows the SV1 mode and the ST1 mode of the suspension bridge computed by GTSTRUDL.

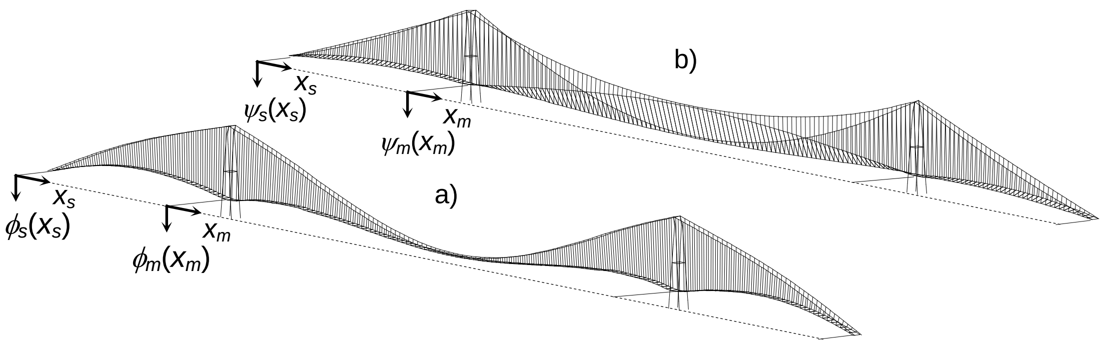

Figure 6. a) 1st symmetric vertical mode (SV1), and
b) 1st symmetric vertical mode (ST1)

The three first SV and ST frequencies are shown in Tables 1, where the results from the CAE and the analytical solution (AM) are compared. The associated analytical mode shapes given in the Appendix are applied in the flutter conditions (19), (20) and (57), (58).

The conditions (19) and (20) are solved graphically using Maple V, see figure 7. The flutter solutions from the suspension bridge conditions and from the sectional

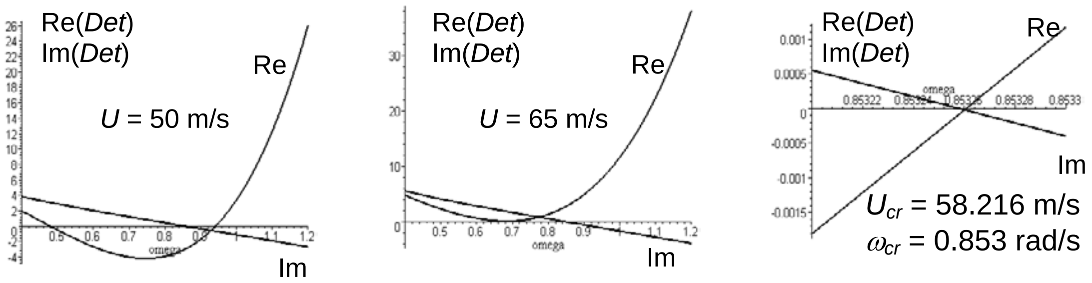

Figure 7. Flutter results from the suspension bridge conditions (21) and (22)

conditions (where $\Phi = \Xi = \Psi$ in (19) and (20)) are compared in Table 2.

Freq.	CAE [rad/s]	AM [rad/s]	Deviation	Freq.	CAE [rad/s]	AM [rad/s]	Deviation
ω_{z1}	0.404	0.402	0.5%	$\omega_{\alpha 1}$	1.276	1.131	11.4%
ω_{z2}	0.630	0.631	0.2%	$\omega_{\alpha 2}$	1.932	2.097	8.5%
ω_{z3}	0.953	0.987	3.6%	$\omega_{\alpha 3}$	2.626	2.416	8.0%

Table 1. Natural vertical and torsional frequencies, 3 first symmetric modes

Freqquency	Suspension bridge	Section	Deviation
U_{cr} [m/s]	58.22	55.85	4.2%
ω_{cr} [rad/s]	0.853	0.878	2.9%

Table 2. Flutter Solutions

6. NUMERICAL ANALYSIS OF SFSC CONDITIONS

The SFSC conditions (57) and (58) are studied for the following varied parameters of the flaps: a) Rotational amplification factors a_{le} and a_{tr}, b) Rotational directions of the flaps, i.e. the signs of a_{le} and a_{tr} (flap configurations), and c) the length of the flaps attached along the girder (Eq. (50)).

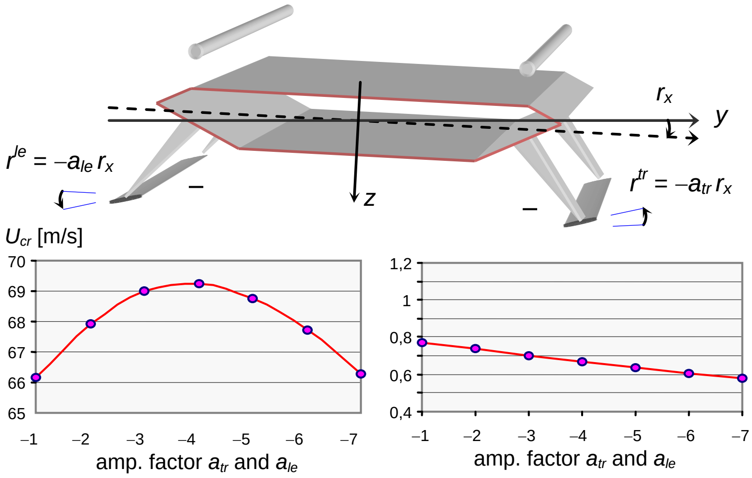

Figure 8. Configuration CMM and full flaps

- *Configuration Minus+Minus (CMM)*: Both of the flaps rotate against the girder. The flap levels in CMM are horizontal if $r^{le} = r^{tr} = -r_x$, which gives an increase in the critical wind speed U_{cr} from 58.1 to 66.2m/s, i.e. 14%. U_{cr} increases until $a_{le} = a_{tr} = -4$ and decreases afterwards. CMM is a good configuration for damping of the torsional vibration of the girder (decreasing critical frequency), figure 8.

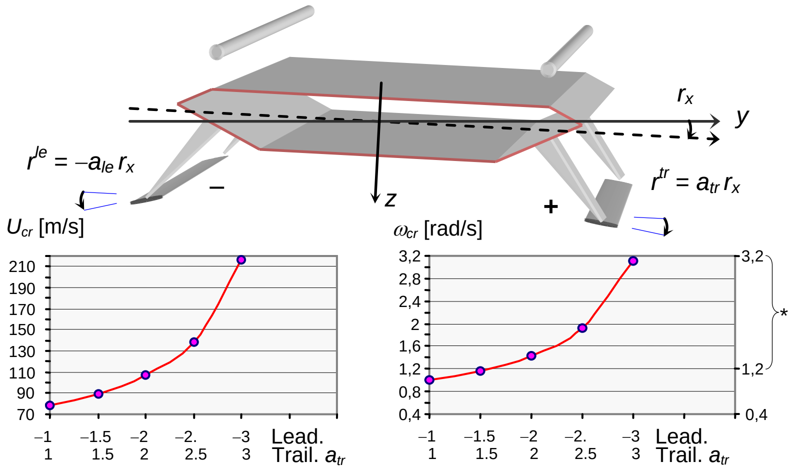

Figure 9. Configuration CMP and full flaps

- *Configuration Minus+Plus (CMP)*: The leading flap rotates against the girder, the trailing flap rotates with the girder. CMP is the most effective configuration against flutter when U_{cr} strongly increases for a small rotation of the flaps. For full flaps in the main span and the side spans, $r^{le} = -1.5r_x$ and $r^{tr} = 1.5r_x$, U_{cr} increases 54% (from 58.1m/s). ω_{cr} increases to the 1st ST frequency and indicate the torsional divergent flutter. By increasing a_{le} and a_{tr} up to –3 and 3, U_{cr} and ω_{cr} can still be found, but ω_{cr} exceeded the 1st ST frequency indicated that higher modes are involved in flutter (control spillover has taken place in the higher modes). The wind speed increase mathematically unlimited without any intersecting the Re(*Det*) and Im(*Det*) on the ω-axis, figure 9.
- *Configuration Plus+Plus (CPP)*: Both of the flaps rotate with the girder. For $r^{le} = r^{tr} = r_x$ the flaps are not rotated relative to the girder. U_{cr} increases 6% (from 58.1m/s), but decreases afterwards for increasing flap rotations. The increasing ω_{cr} shows torsional instability when the leading and the trailing flap are rotated in the same direction with the girder, figure 10.

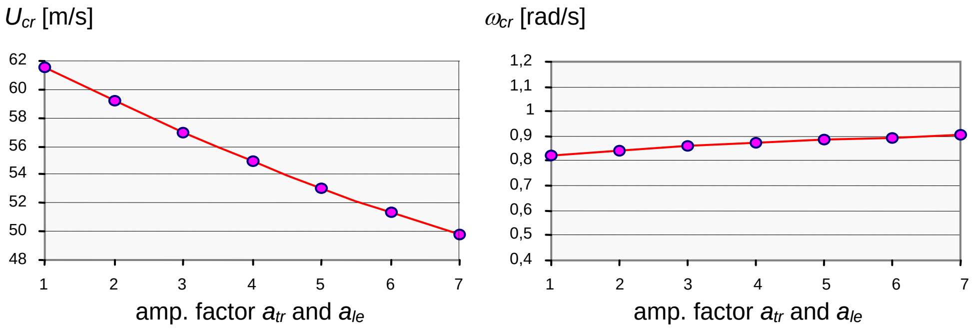

Figure 10. Configuration CPP and full flaps

- *Configuration Plus+Minus (CPM)*: The leading flap rotates with the girder, the trailing flap rotates against the girder. The CPM is the last possible configuration for a simultaneous rotation of both leading and trailing flaps. With this configuration, U_{cr} decreases from the beginning so CPM is an undesirable configuration against the flutter, figure 11.

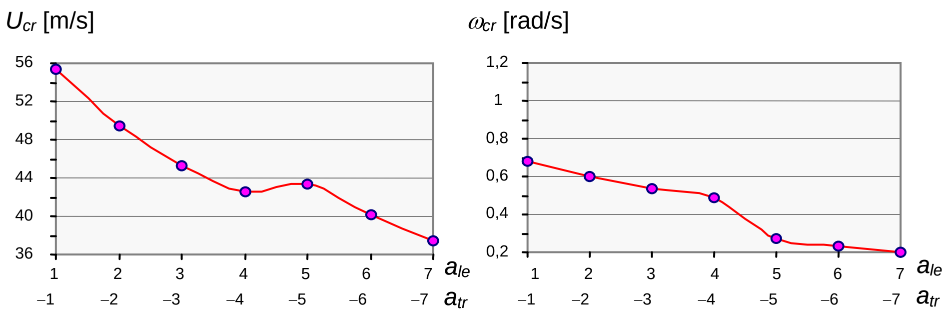

Figure 11. Configuration CPM and full flaps

- *Minimization of the Flaps Length using CMP*: The flap rotations are regulated on the basis of the girder small rotations, which are 2.4° at the flutter velocity 58.2m/s at the center joint of the main span, Huynh [5]. Therefore the flaps rotation can be increased for reducing of the flaps length. In figure 12 the flutter solutions are solved for several combinations of the flap lengths along the center side spans and the main span. The following parameters are fixed: a) 40% and 50% increase of the critical wind speed U_{cr} and b) CMP with leading and trailing flap rotational amplifications of –3 and 3.

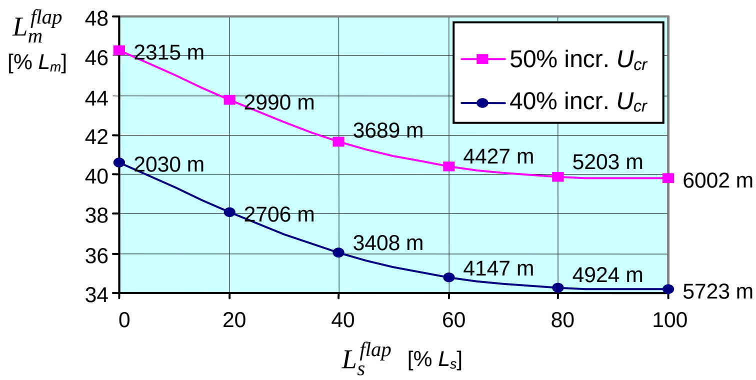

Figure 12. CMP for different combination of flap lengths along the main span center and the side spans center

7. SUMMARY AND CONCLUSION

A suspension bridge of 1000m+2500m+1000m span with separated control flaps has been studied for flutter onset based on the Great Belt girder. A 50% increase of U_{cr} can be obtained for 46 flap sections of dimension 2.7m×25m located along the main span center (of 46% length of the main span). The full flutter period T_f is the oscillations time of the girder from A to C and back to A, FIG. 13. This period is also the sum of the four periods BC, CB, BA and AB. The girder will reach its peak rotation value at C from B in 1.3 seconds at flutter, i.e. the flap rotation within this period is twice the girder rotation r_x. The rotations of the flap away from the center are less because the girder rotations are reduced towards the pylon. The magnitude of the flap rotations ompcared to the girder and the length of the flaps attached along the girder are further presented in the paper.

	Control	No flaps
U_{cr} [m/s]	87.14	58.22
ω_{cr} [rad/s]	1.250	0.853
T_f [sec]	5.03	7.35

Table 3. Flutter for 46% Flaps in the Main Span Center

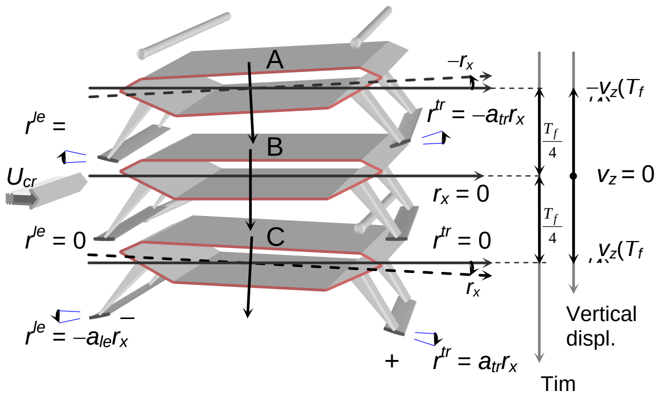

Figure 13. Three vertical positions of the girder and the flaps at flutter
A[$-r_x(T_f/4, x)$, $-v_z(T_f/4, x)$], B [0,0] and C [$r_x(T_f/4, x)$, $v_z(T_f/4, x)$]

Following the increased U_{cr} by using the CMP, the associated critical frequency also increases considerably inasmuch as the control forces have modified the flutter mode (torsional divergent flutter). As long as the desired U_{cr} (and hereby the required control forces) does not produce a higher flutter mode frequency than the ST1 natural frequency, no control spillover takes place in the higher ST modes.

However, at present, the SFSC condition assumes that the forces generated from the girder-wind-interaction and the forces generated from the flap-wind-interaction (for separated flaps) are based on the independent flutter derivatives of the girder and the flaps. The girder-flap interaction (and hereby the new flutter derivatives of the whole system) for a full span model example needs further study in wind tunnel (or by computer simulation) to supplement the assumption of the paper.

APPENDIX. NATURAL MODE SHAPES AND FREQUENCIES OF SUSPENSION BRIDGES

In this appendix the natural mode shapes and frequencies of suspension bridge are outlined analytically, Nielsen & Huynh [6]. The cable mode shape of the main span $\phi_{m,i}(x)$ is:

$$\phi_{m,i}(x) = \frac{1}{\Omega_i^2}\left(1 - \tan\left(\frac{\Omega_i}{2}\right)\sin(\Omega_i \xi) - \cos(\Omega_i \xi)\right) + B_i\left(\xi - \xi^2\right) \qquad (63)$$

where Ω_i = non-dimensional vertical frequency (symmetric) in mode i, $\xi = x/L_m$, x is the coordinate along the main span, and

$$B_i = \frac{b_i}{\Omega_i^2}\left[\frac{\lambda^2}{\Omega_i^2}\left(1-\frac{2}{\Omega_i}\tan\left(\frac{\Omega_i}{2}\right)\right)-\frac{b_i\lambda^2}{6\Omega_i^2}-1\right] \tag{64}$$

$$b_i = \frac{\alpha\,\Omega_i^2}{k(\omega_i)L_m/H - m_p\Omega_i^2/mL_m} \quad , \quad H = mgL_m^2/8f_m \tag{65}$$

$$\alpha = \frac{3}{16}\left(\frac{L_m}{f_m}\right)^2 - \frac{1}{2} \quad , \quad \lambda^2 = \frac{A_cE}{H}\frac{64(f_m/L_m)^2}{1+8(f_m/L_m)^2/3} \tag{66}$$

H is cable horizontal force, m_p is the pylon equivalent mass at the pylon top (assumed to be zero). $k(\Omega_i)$ is the dynamic stiffness of the side span cable of mode i given by

$$k(\Omega_i) = \frac{\lambda_c^2 T}{8f_c}\frac{\Omega_{c,i}^2\cos\theta}{\Omega_{c,i}^2-d_c\lambda_c^2}\cdot\left(\frac{4(f_c/L_c)\alpha_c\cos\theta}{6}-\frac{d_c\sin\theta}{2}\right) \tag{67}$$

where

$$d_c = 1-\frac{2}{\Omega_{c,i}}\tan\frac{\Omega_{c,i}}{2} \quad , \quad \lambda_c^2 = \frac{A_cE}{T}\frac{64(f_c/L_c)^2}{1+8(f_c/L_c)^2/3} \tag{68}$$

$$f_c = \frac{m_c+m_g\cos\theta/2}{m_c+m_g\cos\theta/2}\left(\frac{L_s}{L_m}\right)^2 f_m \quad , \quad \alpha_c = \frac{3}{16}\left(\frac{L_c}{f_c}\right)^2-\frac{1}{2} \tag{69}$$

$$\Omega_{c,i}^2 = \Omega_i^2\frac{m_c+m_g\cos^3\theta/2}{m_c+m_g/2}\left(\frac{L_s}{L_m}\right)^2\frac{1}{\cos\theta} \tag{70}$$

θ is the angle between the chord of the side span cable and horizon. L_c , f_c and T are, respectively, the chord length, the cable sag and the chord force of the side span cable. m_c and m_g is the cable mass (one) and the girder mass per unit span. A_c is the cable area. The dimensionless frequency factor Ω_i is determined iterative by the condition

$$\tan\left(\frac{\Omega_i}{2}\right) = \frac{\Omega_i}{2}-\frac{4}{\lambda^2}\left(\frac{\Omega_i}{2}\right)^3 c(\Omega_i) \tag{71}$$

where

$$c(\Omega_i) = \frac{\lambda^2}{6}\frac{\alpha}{k(\Omega_i)L_m/H - m_p\Omega_i^2/mL_m}+1 \ , \ \omega_i = \Omega_i\sqrt{\frac{H}{mL_m^2}} \tag{72}$$

ω_i is the symmetric vertical frequency of mode i in rad/s.

The side span cable mode shape $\phi_{s,i}(x_c)$ of the bridge vertical mode i can be written in the form

$$\phi_{s,i}(\xi) = C_i\left(1-\tan\left(\frac{\Omega_{c,i}}{2}\right)\sin(\Omega_{c,i}\xi)-\cos(\Omega_{c,i}\xi)\right)+D_i\sin(\Omega_{c,i}\xi) \tag{73}$$

where $\xi = x_c/L_c$, x_c is the coordinate along the chord of the side span cable, and where

$$C_i = \frac{4(f_c/L_c)\alpha_c \cos\theta/6 - d_c \sin\theta/2}{\Omega_c^2 - \lambda_c^2 d_c} \lambda_c^2 X_0^i \quad , \quad D_i = \frac{\sin\theta}{\sin\Omega_{c,i}} X_0^i \tag{74}$$

$$X_0^i = \frac{A_c E}{k(\Omega_i) - \omega_i^2 m_p} \frac{\lambda_m^2 H}{8 f_m} \left[\frac{1}{\Omega_i^2} \left(1 - \frac{2}{\Omega_i} \tan\left(\frac{\Omega_i}{2} \right) \right) - \frac{b_i}{6\Omega_i^2} \right] \tag{75}$$

For ST mode j $\psi_{m,j}(x)$ and $\psi_{s,j}(x)$ are still given by (63) and (73). Ω_j is iterated by the unchanged condition (71), but the girder torsional stiffness is now taking into account in the equation of motion of the cable, Nielsen & Huynh [6].

REFERENCES

[1] Ostenfeld K. H. & Larsen A. “Bridge Engineering and Aerodynamics”, Aerodynamics of Large Bridges – Proceedings of the first International Symposium on Aerodynamics of Large Bridges, Copenhagen/Denmark/19-21 February 1992, Larsen, A. editor, A.A. Balkema Publishers, 1992, pp. 3-22.

[2] Hansen H. I. & P. Thoft-Christensen. “Active Vibration Control of Long Bridges using Flaps”, Presented at Second World Conference on Structural Control, June 28-Juli 1, 1998, Kyoto, Japan.

[3] Hansen H. I. & P. Thoft-Christensen. “Wind Tunnel Experiments with Active Control of Bridge Section Model”, IABSE Reports on IABSE Symposium “Long-Span and High-Rise Structures”, Kobe, Japan, September 2-4, 1998, pp. 199-204.

[4] Hansen H. I. “Active Vibration Control of Long Suspension Bridges”, Ph.D. Thesis, Aalborg University, Aalborg, Denmark, 1998.

[5] Huynh, T. “Suspension Bridge Aerodynamics and Active Vibration Control”, Ph.D. Thesis, Aalborg University, Aalborg, Denmark, 2000.

[6] Nielsen, S. R. K & Huynh, T. “Vibration Theory, Vol. 7A. Special Structures: Aerodynamics of Suspension Bridges”, ISSN 1395-8232 U9902. Aalborg University, Denmark, 1999 (in Danish).

[7] Simiu E. and Scanlan R.H. (“Wind Effects on Structures: Fundamentals and Applications to Design”, Third Edition, John Wiley and Sons, 1996.

[8] Reinhold, T.A., Brinch, M. & Damsgaard, A. “Wind Tunnel Tests for the Great Belt Link”, Danish Maritime Institute, 1992, pp. 255-267.